

Rotational effects on the negative magnetic pressure instability

Illa R. Losada^{1,2}, A. Brandenburg^{3,4}, N. Kleeorin^{5,3}, Dhrubaditya Mitra³, I. Rogachevskii^{5,3}

¹ Department of Astrophysics, Universidad de La Laguna, 38206 La Laguna (Tenerife), Spain

² Instituto de Astrofísica de Canarias, C/ Vía Láctea, s/n, La Laguna, Tenerife, Spain

³ Nordita, Royal Institute of Technology and Stockholm University, Roslagstullsbacken 23, 10691 Stockholm, Sweden

⁴ Department of Astronomy, AlbaNova University Center, Stockholm University, 10691 Stockholm, Sweden

⁵ Department of Mechanical Engineering, Ben-Gurion University of the Negev, POB 653, Beer-Sheva 84105, Israel

July 24, 2012, Revision: 1.107

ABSTRACT

Context. The surface layers of the Sun are strongly stratified. In the presence of turbulence with a weak mean magnetic field, a large-scale instability resulting in the formation of non-uniform magnetic structures, can be excited over the scale of many turbulent eddies or convection cells. This instability is caused by a negative contribution of turbulence to the effective (mean-field) magnetic pressure and has previously been discussed in connection with the formation of active regions and perhaps sunspots.

Aims. We want to understand the effects of rotation on this instability in both two and three dimensions.

Methods. We use mean-field magnetohydrodynamics in a parameter regime in which the properties of the negative effective magnetic pressure instability have previously been found to be in agreement with those of direct numerical simulations.

Results. We find that the instability is suppressed already for relatively slow rotation with Coriolis numbers (i.e. inverse Rossby numbers) around 0.2. The suppression is strongest at the equator. In the nonlinear regime, we find traveling wave solutions with propagation in the prograde direction at the equator with additional poleward migration away from the equator.

Conclusions. The prograde rotation of the magnetic pattern near the equator is argued to be a possible explanation for the faster rotation speed of magnetic tracers found on the Sun. In the bulk of the domain, kinetic and current helicities are negative in the northern hemisphere and positive in the southern.

Key words. magnetohydrodynamics (MHD) – hydrodynamics – turbulence – Sun: dynamo

1. Introduction

In the outer parts of the Sun, energy is transported through turbulent convection. The thermodynamic aspects of this process are well understood through mixing length theory (Vitense, 1953). Also reasonably well understood is the partial conversion of kinetic energy into magnetic energy via dynamo action (Parker, 1979; Zeldovich et al., 1983). Most remarkable is the possibility of generating magnetic fields on scales much larger and much longer than those of the turbulence itself. This has now been seen in many three-dimensional turbulence simulations (Brandenburg, 2001; Brandenburg & Subramanian, 2005), but the physics of this is best understood in terms of mean-field theory, which encapsulates the effects of complex motions in terms of effective equations for mean flow and mean magnetic field (Moffatt, 1978; Parker, 1979; Krause & Rädler, 1980).

The effects of stratification are usually only included to leading order and often only in connection with rotation, because the two together give rise to the famous α effect, which is able to explain the generation of large-scale magnetic fields (Krause & Rädler, 1980). In recent years, however, a completely different effect arising from strong stratification alone has received attention: the suppression of turbulent pressure by a weak mean magnetic field. This effect mimics a negative effective (mean-field) magnetic pressure due to a negative contribution of

turbulence to the mean magnetic pressure. Under suitable conditions, this leads to the negative effective magnetic pressure instability (NEMPI) which can cause the formation of magnetic flux concentrations. In turbulence simulations, this instability has been seen only recently (Brandenburg et al., 2011), because significant scale separation is needed to overcome the effects of turbulent diffusion (Brandenburg et al., 2012). Mean-field considerations, however, have predicted the existence of NEMPI for a long time (Kleeorin et al., 1989, 1990; Kleeorin & Rogachevskii, 1994; Kleeorin et al., 1996; Rogachevskii & Kleeorin, 2007; Brandenburg, Kleeorin, & Rogachevskii, 2010).

Despite the potential importance of NEMPI, many additional effects have not yet been explored. The idea is that NEMPI would interact with the global dynamo producing the large-scale magnetic field for NEMPI to act upon. Thus, the field needs to be self-consistently generated. Ideally, global geometry is needed, and such calculations should be three-dimensional (3-D), because one expects flux concentrations not to be two-dimensional (2-D) or axisymmetric. New mean-field coefficients will appear in such a more general case, and not much is known about those coefficients. Nevertheless, although other terms may appear, it will be interesting to investigate the evolution of NEMPI in more realistic cases with just the leading term responsible for the instability.

The purpose of the present paper is to include the effects of rotation as it appears in a local Cartesian domain at a given latitude in the Sun. Our main goal is to determine the dependence of growth rate and saturation level of NEMPI on rotation rate and latitude, and to characterize rotational effects on the resulting flux concentrations. For the purpose of this work, we restrict ourselves in the following to a mean-field treatment and denote averaged quantities by an overbar. Furthermore, we make the assumption of an isothermal equation of state. This is of course quite unrealistic, as far as applications to the Sun is concerned. However, it has been found earlier that NEMPI has similar properties both for an isothermal layer with an isothermal equation of state as well as a nearly isentropic one with the more general perfect gas law (Käpylä et al., 2012). Given that our knowledge of NEMPI is still rather limited, it is useful to consider the new effects of rotation within the framework of the conceptually simpler case of an isothermal layer.

One of the remarkable insights is that NEMPI can occur at any depth, depending just on the value of the mean magnetic field strength. However, for a domain of given depth extent, the instability can only occur if the location where the dependence of effective turbulent pressure on the ratio field strength to equipartition value has a negative slope. Once this is obeyed, the only other necessary condition for NEMPI to occur is that the turbulent diffusivity is small enough. In practice this means that there are sufficiently many turbulent eddies within the domain of investigation (Brandenburg et al., 2012; Kemel et al., 2012b).

We begin with the model equations, present then first the linear theory of NEMPI in the presence of rotation, and consider then two- and three-dimensional numerical models.

2. The model

We consider here an isothermal equation of state with constant sound speed c_s , so the mean pressure is $\bar{p} = \bar{\rho}c_s^2$. The evolution equations for mean velocity $\bar{\mathbf{U}}$, mean density $\bar{\rho}$, and mean vector potential $\bar{\mathbf{A}}$, are

$$\frac{D\bar{\mathbf{U}}}{Dt} = -2\boldsymbol{\Omega} \times \bar{\mathbf{U}} - c_s^2 \nabla \ln \bar{\rho} + \mathbf{g} + \bar{\mathcal{F}}_M + \bar{\mathcal{F}}_K, \quad (1)$$

$$\frac{D\bar{\rho}}{Dt} = -\bar{\rho} \nabla \cdot \bar{\mathbf{U}}, \quad (2)$$

$$\frac{\partial \bar{\mathbf{A}}}{\partial t} = \bar{\mathbf{U}} \times \bar{\mathbf{B}} - (\eta_t + \eta) \bar{\mathbf{J}}, \quad (3)$$

where $D/Dt = \partial/\partial t + \bar{\mathbf{U}} \cdot \nabla$ is the advective derivative, $\mathbf{g} = (0, 0, -g)$ is the acceleration due to the gravity field,

$$\bar{\mathcal{F}}_K = (\nu_t + \nu) (\nabla^2 \bar{\mathbf{U}} + \frac{1}{3} \nabla \nabla \cdot \bar{\mathbf{U}} + 2 \bar{\mathbf{S}} \nabla \ln \bar{\rho}) \quad (4)$$

is the total (turbulent plus microscopic) viscous force, and $\bar{\mathcal{S}}_{ij} = \frac{1}{2}(\bar{U}_{i,j} + \bar{U}_{j,i}) - \frac{1}{3}\delta_{ij} \nabla \cdot \bar{\mathbf{U}}$ is the traceless rate of strain tensor of the mean flow. The mean Lorentz force, $\bar{\mathcal{F}}_M$, is given by

$$\bar{\rho} \bar{\mathcal{F}}_M = \bar{\mathbf{J}} \times \bar{\mathbf{B}} + \frac{1}{2} \nabla (q_p \bar{B}^2), \quad (5)$$

where $\bar{\mathbf{J}} = \nabla \times \bar{\mathbf{B}}/\mu_0$ is the mean current density, μ_0 is the vacuum permeability, and the last term, $\frac{1}{2} \nabla (q_p \bar{B}^2)$,

on the right hand side of Equation (5) determines the turbulent contribution to the mean Lorentz force. Following Brandenburg et al. (2012) and Kemel et al. (2012a), the function $q_p(\beta)$ is approximated by:

$$q_p(\beta) = \frac{\beta_\star^2}{\beta_p^2 + \beta^2}, \quad (6)$$

where β_\star and β_p are constants, $\beta = \bar{B}/B_{\text{eq}}$ is the modulus of the normalized mean magnetic field, and $B_{\text{eq}} = \sqrt{\mu_0 \bar{\rho}} u_{\text{rms}}$ is the equipartition field strength. The angular velocity vector $\boldsymbol{\Omega}$ is quantified by its scalar amplitude Ω and colatitude θ , such that

$$\boldsymbol{\Omega} = \Omega (-\sin \theta, 0, \cos \theta). \quad (7)$$

In this arrangement, z corresponds to radius, x to colatitude, and y to azimuth.

Following the simplifying assumption of recent direct numerical simulations of NEMPI (Brandenburg et al., 2011), we assume that the root-mean-square turbulent velocity, u_{rms} , is constant in space and time. For an isothermal density stratification,

$$\bar{\rho} = \rho_0 \exp(-z/H_\rho), \quad (8)$$

where $H_\rho = c_s^2/g$ is the density scale height, we then have $B_{\text{eq}}(z)$. To quantify the strength of the imposed field, we also define $B_{\text{eq}0} = B_{\text{eq}}(z=0)$. The value of u_{rms} is also related to the values of η_t and ν_t , which we assume to be equal, with $\eta_t = \nu_t = u_{\text{rms}}/3k_f$, where k_f is the wavenumber of the energy-carrying eddies of the underlying turbulence. This formula assumes that the relevant correlation time is $(u_{\text{rms}}k_f)^{-1}$, which turns out to be fairly accurate (Sur et al., 2008).

3. Linear theory of NEMPI with rotation

In this section we study the effect of rotation on the growth rate of NEMPI. Following earlier work (e.g., the appendix of Kemel et al., 2012b), we neglect for simplicity dissipation processes, use the anelastic approximation, $\nabla \cdot \bar{\rho} \bar{\mathbf{U}} = 0$, and assume that the density scale height $H_\rho = \text{const}$. We consider the equation of motion, ignoring the $\bar{\mathbf{U}} \cdot \nabla \bar{\mathbf{U}}$ non-linearity,

$$\frac{\partial \bar{\mathbf{U}}(t, x, z)}{\partial t} = -2\boldsymbol{\Omega} \times \bar{\mathbf{U}} - \frac{1}{\bar{\rho}} \nabla p_{\text{tot}} + \mathbf{g}, \quad (9)$$

where $p_{\text{tot}} = \bar{p} + p_{\text{eff}}$ is the total pressure consisting of the sum of the mean gas pressure \bar{p} , and the effective magnetic pressure, $p_{\text{eff}} = (1 - q_p) \bar{B}^2/2$, where $\bar{\mathbf{B}} = |\bar{\mathbf{B}}|$. Here and elsewhere the vacuum permeability is set to unity. Let us assume for simplicity that $\partial_y = 0$, and that the mean magnetic field has only a y -component, $\bar{\mathbf{B}} = (0, \bar{B}_y(x, z), 0)$, so the mean magnetic tension, $\bar{\mathbf{B}} \cdot \nabla \bar{\mathbf{B}}$ in Equation (9) vanishes.

Taking twice the curl of Equation (9), and noting further that $\hat{\mathbf{z}} \cdot \nabla \times \nabla \times \bar{\mathbf{U}} = -\Delta \bar{U}_z + \nabla_z \nabla \cdot \bar{\mathbf{U}}$, we obtain

$$\begin{aligned} \frac{\partial}{\partial t} [\Delta \bar{U}_z + \nabla_z (\bar{\mathbf{U}} \cdot \nabla \ln \bar{\rho})] &= -2\boldsymbol{\Omega} \cdot \nabla (\nabla \times \bar{\mathbf{U}})_z \\ &+ \nabla_x \left[\left(\nabla_z \frac{p_{\text{tot}}}{\bar{\rho}} \right) \frac{\nabla_x \bar{\rho}}{\bar{\rho}} - \left(\nabla_x \frac{p_{\text{tot}}}{\bar{\rho}} \right) \frac{\nabla_z \bar{\rho}}{\bar{\rho}} \right], \end{aligned} \quad (10)$$

where we have used the anelastic approximation in the form $\nabla \cdot \bar{\mathbf{U}} = -\bar{\mathbf{U}} \cdot \nabla \ln \bar{\rho}$ and the fact that under the curl the gradient can be moved to $\bar{\rho}$. We have also taken into account that $\Omega_y = 0$ and have used Eq. (30) of Kemel et al. (2012b) to relate the double-curl of $(\nabla p_{\text{tot}})/\bar{\rho}$ to the last term in Equation (10). The first term on the right hand side of Equation (10) for \bar{U}_z is proportional to $(\nabla \times \bar{\mathbf{U}})_z$. Taking the z component of the curl of Equation (9) we obtain the following equation for $(\nabla \times \bar{\mathbf{U}})_z$:

$$\frac{\partial}{\partial t}(\nabla \times \bar{\mathbf{U}})_z = 2 \left(\Omega \cdot \nabla - \frac{\Omega_z}{H_\rho} \right) \bar{U}_z. \quad (11)$$

The induction equation for $\bar{B}_y(x, z)$ is given by

$$\frac{D\bar{B}_y}{Dt} = -\bar{B}_y \nabla \cdot \bar{\mathbf{U}}, \quad (12)$$

where $D/Dt = \partial/\partial t + \bar{\mathbf{U}} \cdot \nabla$ is the advective derivative. Note that for a magnetic field with only a y -component, but $\partial/\partial y = 0$, there is no stretching term, so there is no term of the form $\bar{\mathbf{B}} \cdot \nabla \bar{\mathbf{U}}$.

We linearize Equations (10)–(12), indicating small changes by δ . We consider an equilibrium with a constant magnetic field of the form $(0, B_0, 0)$, a zero mean velocity and the fluid density is given by Equation (8). We take into account that the function $q_p = q_p(\beta)$ depends both on \bar{B} and on $\bar{\rho}$, which implies that (Kemel et al., 2012b)

$$\delta \left(\frac{p_{\text{tot}}}{\bar{\rho}} \right) = \frac{1}{2} v_A^2 \left(1 - q_p - \frac{dq_p}{d \ln \beta^2} \right) \left(2 \frac{\delta \bar{B}_y}{B_0} - \frac{\delta \bar{\rho}}{\bar{\rho}} \right), \quad (13)$$

while

$$\nabla_z \left(\frac{p_{\text{tot}}}{\bar{\rho}} \right) = \frac{1}{2} v_A^2 \left(1 - q_p - \frac{dq_p}{d \ln \beta^2} \right) \frac{1}{H_\rho}. \quad (14)$$

The linearized system of equations reads:

$$\frac{\partial}{\partial t} \left(\Delta - \frac{1}{H_\rho} \nabla_z \right) \delta \bar{U}_z = 2 \frac{v_A^2}{H_\rho} \frac{d\mathcal{P}_{\text{eff}}}{d\beta^2} \frac{\nabla_x^2 \delta \bar{B}_y}{B_0} - 2\Omega \cdot \nabla (\nabla \times \delta \bar{\mathbf{U}})_z, \quad (15)$$

$$\frac{\partial}{\partial t} (\nabla \times \delta \bar{\mathbf{U}})_z = 2 \left(\Omega \cdot \nabla - \frac{\Omega_z}{H_\rho} \right) \delta \bar{U}_z, \quad (16)$$

$$\frac{\partial \delta \bar{B}_y}{\partial t} = -B_0 \frac{\delta \bar{U}_z}{H_\rho}, \quad (17)$$

where $\mathcal{P}_{\text{eff}}(\beta) = \frac{1}{2} [1 - q_p(\beta)] \beta^2$ is the effective magnetic pressure normalized by the local value of B_{eq}^2 .

Introducing a new variable $V_z = \sqrt{\bar{\rho}} \delta \bar{U}_z$ in Equations (15)–(17) and after simple transformations we arrive at the following equation for one variable V_z :

$$\frac{\partial^2}{\partial t^2} \left(\Delta - \frac{1}{4H_\rho^2} \right) V_z + \left((2\Omega \cdot \nabla)^2 - \frac{\Omega_z^2}{H_\rho^2} \right) V_z = \lambda_0^2 \nabla_x^2 V_z, \quad (18)$$

where

$$\lambda_0^2(z) = -2 \frac{v_A^2(z)}{H_\rho^2} \frac{d\mathcal{P}_{\text{eff}}(z)}{d\beta^2}. \quad (19)$$

In the WKB approximation, which is valid when $k_z H_\rho \gg 1$, i.e., when the characteristic scale of the spatial

variation of the perturbations of the magnetic and velocity fields are much smaller than the density height length, H_ρ , the growth rate of the large-scale instability is given by

$$\lambda = \left[\lambda_0^2 \frac{k_x^2}{k^2} - \omega_{\text{inert}}^2 \right]^{1/2}, \quad (20)$$

where $\omega_{\text{inert}} = 2\Omega \cdot \hat{\mathbf{k}}$ is the frequency of the inertial waves. Here, $\hat{\mathbf{k}} = \mathbf{k}/k$ is the unit vector of \mathbf{k} . Note that λ is either real or purely imaginary, so no complex eigenvalues are possible, as would be required for growing oscillatory solutions. Without rotation the growth rate of the large-scale instability (NEMPI) is (Kleorin et al., 1993; Rogachevskii & Kleorin, 2007; Kemel et al., 2012c)

$$\lambda = \frac{v_A}{H_\rho} \left(-2 \frac{d\mathcal{P}_{\text{eff}}}{d\beta^2} \right)^{1/2} \frac{k_x}{k}, \quad (21)$$

and a necessary condition for the instability is

$$\frac{d\mathcal{P}_{\text{eff}}}{d\beta^2} < 0. \quad (22)$$

NEMPI can be excited even in a uniform mean magnetic field, and the source of free energy of the instability is provided by the small-scale turbulence. In contrast, the free energy in Parker's magnetic buoyancy instability (Parker, 1966) or in the interchange instability (Tserkovnikov, 1960; Priest, 1982) is drawn from the gravitational field. Both instabilities are excited in a plasma when the characteristic scale of variations of the original horizontal magnetic field is smaller than the density scale height.

The rotation reduces the growth rate of NEMPI, that can be excited when $k_x/k > \omega_{\text{inert}}/\lambda_0$ and $d\mathcal{P}_{\text{eff}}/d\beta^2 < 0$. In opposite case, $k_x/k < \omega_{\text{inert}}/\lambda_0$, the large-scale instability is not excited, while the frequency of the inertial waves is reduced due to the effective negative magnetic pressure.

For an arbitrary vertical inhomogeneity of the density, we seek a solution of Equation (18) in the form $V_z(t, x, z) = V(z) \exp(\lambda t + i k_x x)$ and obtain an eigenvalue problem

$$\left[\nabla_z^2 + \frac{8\Omega_x \Omega_z}{\lambda^2 + 4\Omega_z^2} i k_x \nabla_z - \Lambda^2 k_x^2 - \frac{1}{4H_\rho^2} \right] V(z) = 0, \quad (23)$$

where

$$\Lambda^2 = \frac{\lambda^2 - \lambda_0^2(z) + 4\Omega_x^2}{\lambda^2 + 4\Omega_z^2}, \quad (24)$$

and λ is the eigenvalue. Equation (23) can be reduced to the Schrödinger type equation, $\Psi'' - \tilde{U}(R) \Psi = 0$, via the transformation

$$\Psi(R) = \sqrt{R} V(z) \exp \left(i \frac{4\Omega_x \Omega_z}{\lambda^2 + 4\Omega_z^2} k_x z \right), \quad (25)$$

$$R(z) = \frac{v_{A0}^2}{u_{\text{rms}}^2 \beta_p^2} e^{z/H_\rho}, \quad (26)$$

where $v_{A0} = B_0/\sqrt{\bar{\rho}_0}$ is the Alfvén speed based on the averaged density, the potential $\tilde{U}(R)$ is

$$\tilde{U}(R) = \frac{k_x^2 H_\rho^2}{R(\lambda^2 + 4\Omega_z^2)} \left[\frac{\lambda^2}{R} \left(\frac{\lambda^2 + 4\Omega_z^2}{\lambda^2 + 4\Omega_z^2} \right) + \frac{u_{\text{rms}}^2 \beta_p^2}{H_\rho^2} \left(1 - \frac{q_{p0}}{(1+R)^2} \right) \right], \quad (27)$$

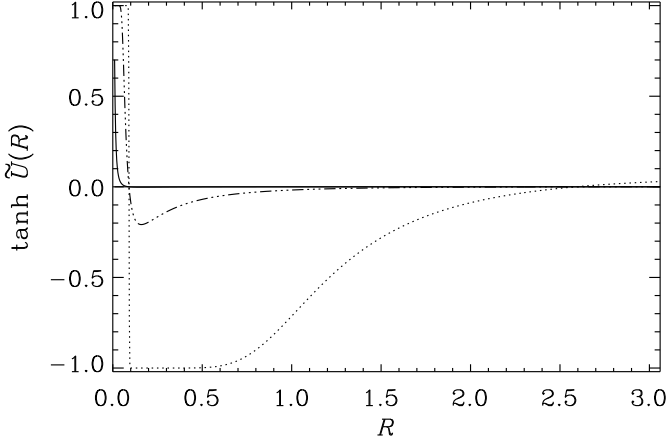


Fig. 1. $\tanh \tilde{U}(R)$ for $\tilde{\lambda} = 0.02$, $\theta = 0$ and $\Omega = 0.01, 0.1$, and 1 .

and we have used Equation (6) for q_p with $\beta_\star = \beta_p \sqrt{q_{p0}}$ and $q_{p0} = q_p(\beta = 0)$. As follows from Equation (27), the potential, $\tilde{U}(R)$, is positive for $R \rightarrow 0$ and $R \rightarrow \infty$. Therefore, for the existence of the instability, the potential should have a negative minimum. This is possible, when $q_{p0} > (1 + R)^2$. When the potential $\tilde{U}(R)$ has a negative minimum, there are two points R_1 and R_2 (the so-called turning points) in which $\tilde{U}(R = R_{1,2}) = 0$. Figure 1 shows $\tanh \tilde{U}(R)$ for different values of Ω . This representation allows us to distinguish better the behavior for small values of $\tilde{U}(R)$.

Using Equation (27) and the condition $\tilde{U}(R = R_{1,2}) = 0$, we estimate the maximum growth rate of the instability as

$$\lambda = \frac{1}{\sqrt{2}} \left[\lambda_\star^2 - 4\Omega^2 + [(\lambda_\star^2 - 4\Omega^2)^2 + 8\Omega_z^2 \lambda_\star^2]^{1/2} \right]^{1/2}, \quad (28)$$

where

$$\lambda_\star = \frac{\beta_\star u_{\text{rms}}}{H_\rho} \frac{[R_1 R_2 (2 + R_1 + R_2)]^{1/2}}{(1 + R_1)(1 + R_2)}. \quad (29)$$

By defining $\sigma = 4\Omega^2/\lambda_\star^2$, Equation (28) can also be written as

$$\lambda/\lambda_\star = \frac{1}{\sqrt{2}} \left[1 - \sigma + (1 - 2\sigma \sin^2 \theta + \sigma^2)^{1/2} \right]^{1/2}. \quad (30)$$

Note that for $\sigma \gg 1$, we obtain that $\lambda/\lambda_\star = \cos \theta$, which is independent of the value of σ . In Figure 2 we plot the dependence of λ/λ_\star on θ for different values of σ . This analytic result shows that, if λ_\star were independent of θ , the growth rate remains unaffected by rotation at the poles, and is suppressed near the equator for $\Omega = O(\lambda_\star)$.

Unfortunately, the analytic result does not allow an easy inspection concerning the sign of the frequency and hence the direction of the travelling wave solutions. Therefore we turn in the following to numerical simulations of the full 2-D and 3-D mean-field equations.

4. Numerical Results

In this section we discuss numerical mean-field modelling. We consider a computational domains of size L^2 or L^3

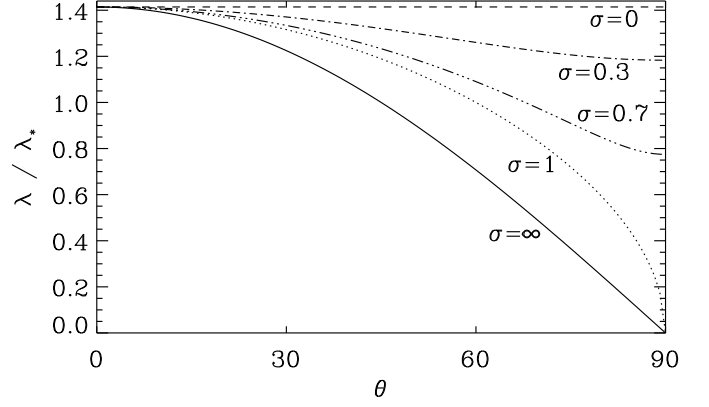


Fig. 2. Theoretical dependence of λ/λ_\star on θ for different values of σ .

with periodic boundary conditions in the horizontal direction(s) and stress-free perfect conductor boundary conditions in the vertical direction. The smallest wavenumber that fits horizontally into the domain has the wavenumber $k_1 = 2\pi/L$. The numerical simulations are performed with the PENCIL CODE¹, which uses sixth-order explicit finite differences in space and a third-order accurate time stepping method (Brandenburg & Dobler, 2002). As units of length we use k_1^{-1} and time is measured in units of $(c_s k_1)^{-1}$. For the models presented below, we use $q_{p0} = 20$ and $\beta_p = 0.167$, which corresponds to $\beta_\star = 0.75$, and is appropriate for the parameter regime in which $R_m \approx 18$ and $k_f/k_1 = 30$ (Kemel et al., 2012c).

An important non-dimensional parameter is the Coriolis number, $\text{Co} = 2\Omega/u_{\text{rms}}k_f$. Using $k_f = u_{\text{rms}}/3\eta_t$, we can express this in terms of the parameter $C_\Omega = \Omega/\eta_t k_1^2$, which is often used in mean-field dynamo theory. Thus, we have

$$\text{Co} = 6\eta_t \Omega / u_{\text{rms}}^2 = 6(\eta_t k_1 / u_{\text{rms}})^2 C_\Omega. \quad (31)$$

Motivated by the analytic results of the previous section we normalize the growth rate of the instability alternatively by a quantity $\lambda_{\star 0} \equiv \beta_\star u_{\text{rms}}/H_\rho$. In the following we take $u_{\text{rms}}/c_s = 0.1$. Further, we use $\nu_t = \eta_t = 10^{-3}c_s/k_f$, so that $k_f H_\rho \approx 33$ and $\eta_t k_1 / u_{\text{rms}} = 10^{-2}$. This also means that for $\Omega = 0.01$, for example, we have $2\Omega/\lambda_{\star 0} = 0.27$ and $\text{Co} = 0.006$.

We use either $B_0/B_{\text{eq}0} = 0.1$ or 0.05 . We recall, however, that the growth rate does not depend on this choice, provided the bulk of the eigenfunction fits into the domain, which is here the case for both values of B_0 . (For the smaller value of B_0 the maximum of the magnetic structures (i.e., the maximum of the eigenfunction in z) is slightly higher up in the domain, but in both cases the maximum is contained within the domain.)

We discuss first the Ω and θ dependence of 2-D and 3-D solutions. Using $\theta = 0^\circ, 45^\circ$, and 90° , corresponding to $90^\circ, 45^\circ$, and 0° latitude, we find that NEMPI is suppressed for rotation rates around $\Omega \approx 0.01c_s k_1$ and 0.025 in 2-D and 3-D, as can be seen in Figures 3 and 4. This corresponds to $\text{Co} = 0.006$ and 0.015 , which are remarkably small values. Note the similar behavior in 2-D and 3-D: NEMPI is suppressed for even smaller values of $2\Omega/\lambda_{\star 0}$ as θ increases.

¹ <http://pencil-code.googlecode.com>

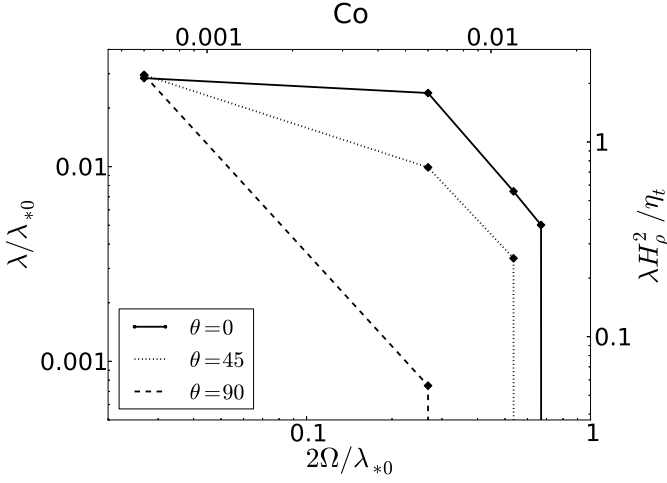


Fig. 3. Dependence of λ/λ_{*0} on $2\Omega/\lambda_{*0}$ for three values of θ for 2-D simulations with $B_0/B_{\text{eq}0} = 0.1$.

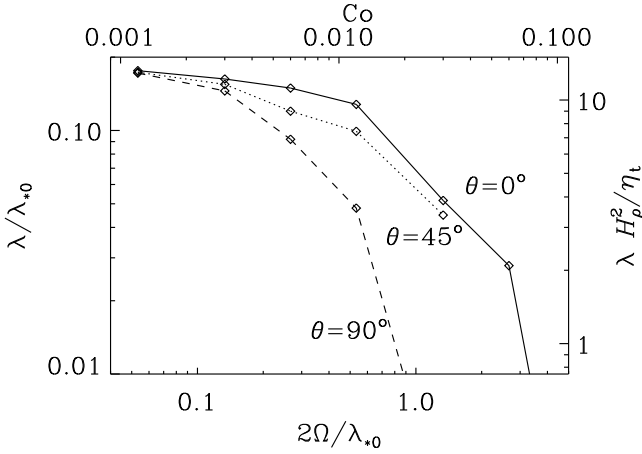


Fig. 4. Dependence of λ/λ_{*0} on $2\Omega/\lambda_{*0}$ for three values of θ for three-dimensional simulations with $B_0/B_{\text{eq}0} = 0.05$.

Next, we vary θ . As expected from the results of Section 3, and as already seen in Figures 3 and 4, the largest growth rates occur at the poles ($\theta = 0$), and NEMPI is most strongly suppressed at the equator. The growth rate as a function of θ is given in Figure 5 for two values of $2\Omega/\lambda_{*0}$, showing a minimum at $\theta = 90^\circ$ (i.e., at the equator). In the upper panel of Figure 5, we have used two-dimensional results, i.e. we have restricted ourselves to solutions with $\partial/\partial y = 0$, as was also done in Section 3. However, this is only an approximation to the fully three-dimensional case. The usefulness of this restriction can be assessed by comparing two-dimensional and three-dimensional results; see the lower panel of Figure 5. While the θ dependence is roughly similar in the two- and three-dimensional cases, the growth rates are by at least a factor of two smaller in the two-dimensional case.

To determine the oscillatory frequency of the growing mode, we consider the values of $u_y(\mathbf{x}_1, t)$ and $B_y(\mathbf{x}_1, t)$ at a fixed point. To determine the oscillatory frequency, we consider the values of $\bar{U}_y(\mathbf{x}_1, t)$ and $\bar{B}_y(\mathbf{x}_1, t)$ at a fixed point \mathbf{x}_1 within the domain. As can be seen in Figures 6

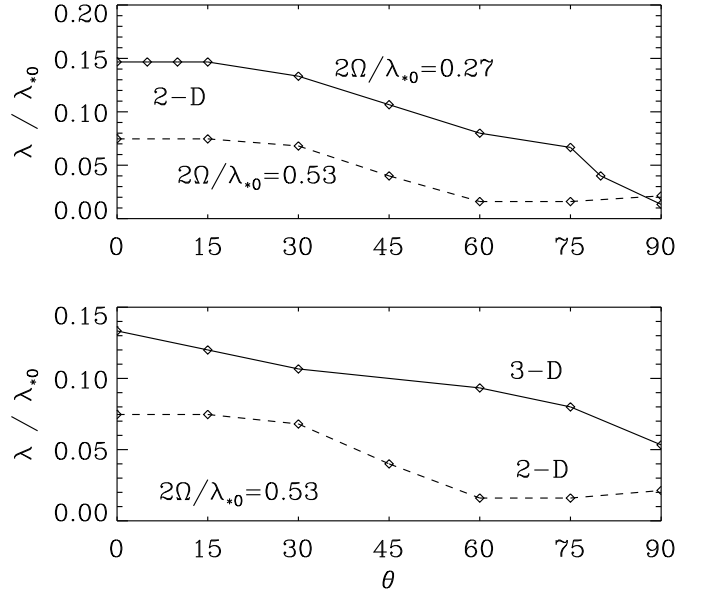


Fig. 5. Dependence of λ/λ_{*0} on θ for two values of $2\Omega_0/\lambda_{*0}$ in 2-D (upper panel) and comparison of 2-D and 3-D cases (lower panel).

and 7, their frequency and amplitude depend both on Ω and θ . The oscillations are not always harmonic ones, and can be irregular with variable periods, making the period determination more difficult. Nevertheless, the frequencies for \bar{U}_y and \bar{B}_y are similar over broad parameter ranges, as is expected from linear theory. For $\Omega_0/\lambda_{*0} > 0.25$ at $\theta = 60^\circ$, NEMPI is no longer excited, but there are still oscillations in $u_y(\mathbf{x}_1, t)$ which must then have some other reason.

We find a substantial variation of the amplitude for the values of maximum growing rate for $\Omega = 0.01$ and $\Omega = 0.02$. (Note that the high frequency in u_y and B_y in Figure 6 corresponds to a random small-amplitude change.) The frequency of the oscillations is very small at the poles, but it reaches a maximum at $\theta = 45$ and decreases again toward the equator.

Given the combined presence of rotation and stratification, we expect the resulting velocity and magnetic fields to be helical. We plot in the upper panel of Figure 8 relative kinetic, current, and cross helicities. These are here abbreviated in terms of the function

$$\mathcal{H}(\mathbf{p}, \mathbf{q}) = \langle \mathbf{p} \cdot \mathbf{q} \rangle / \sqrt{\langle \mathbf{p}^2 \rangle \langle \mathbf{q}^2 \rangle}, \quad (32)$$

where \mathbf{p} and \mathbf{q} are two arbitrary vectors. Here, $\langle \cdot \rangle$ denotes xy averaging. Note that the relative kinetic helicity, $\mathcal{H}(\bar{\mathbf{W}}, \bar{\mathbf{U}})$, where $\bar{\mathbf{W}} = \nabla \times \bar{\mathbf{U}}$ is the mean vorticity, varies between nearly +1 in the lower part and −1 in the upper part. This change of sign is familiar from laminar convection where upwellings expand to produce negative helicity in the upper parts, and downwellings also expand as they hit the bottom of the domain (e.g. Brandenburg et al., 1990). However, in the lower part of the domain both $\bar{\mathbf{U}}$ and $\bar{\mathbf{W}}$ are relatively small, as can be seen by considering their relative amplitudes, $\mathcal{A}(\bar{\mathbf{U}})$ and $\mathcal{A}(\bar{\mathbf{W}})$, where

$$\mathcal{A}(\mathbf{p}) = \langle \mathbf{p}^2 \rangle / \langle \langle \mathbf{p}^2 \rangle \rangle, \quad (33)$$

with $\langle \langle \cdot \rangle \rangle$ being defined as volume averages.

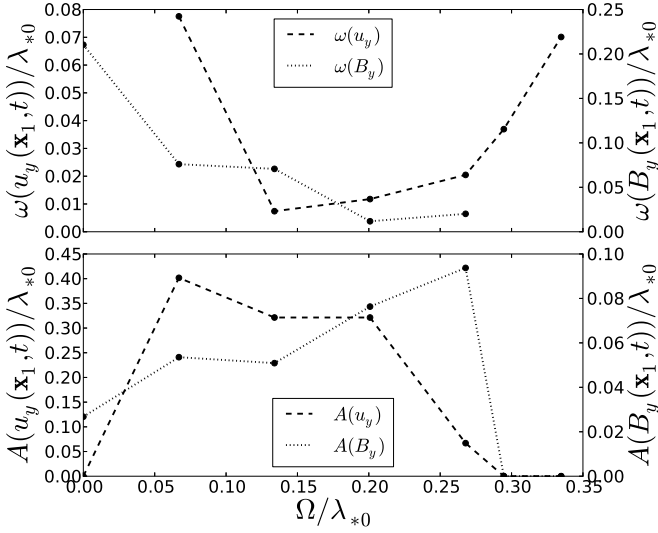


Fig. 6. Frequency and amplitude as a function of Ω for $\theta = 60^\circ$ and $B_0/B_{\text{eq}0} = 0.1$ in the saturated regime.

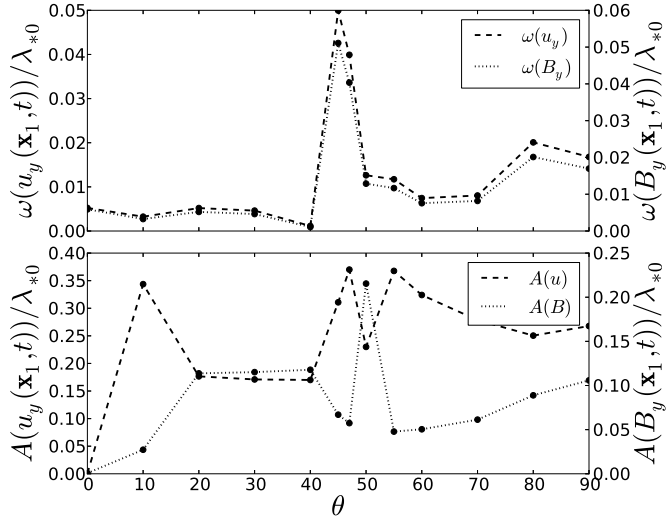


Fig. 7. Frequency and amplitude θ dependence for $\Omega = 0.01$ and $B_0/B_{\text{eq}0} = 0.1$.

Finally, let us turn to the spatial structure of NEMPI. In Figure 9 we compare \bar{B}_y at different times and latitudes for the 2-D runs. Note that in the exponentially growing phase of NEMPI, the structures do not propagate (or move only very slowly). Traveling wave solutions occur mainly in later stage of NEMPI, i.e., in the saturated regime. Next, we consider the 3-D case. In Figure 10 we show visualizations of the magnetic field on the periphery of the computational domain for 4 different times for $\theta = 0$. Note that magnetic structures are inclined in the xy plane. This is a direct result of rotation. As expected, the inclination is for negative values of Ω ; see Figure 11. The inclination angle is about 30° , corresponding to 0.5 radians, which is not compatible with the value of $\text{Co} \approx 0.03$, but it is closer to the value of $\Omega/\lambda_{*0} \approx 0.65$. However, in this connection we should stress that we have imposed periodic boundary conditions in the

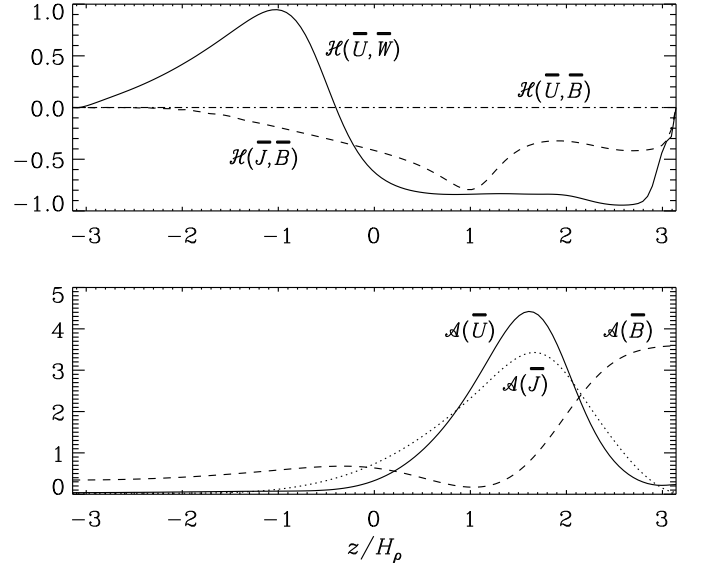


Fig. 8. Dependence of various relative helicities and relative amplitudes on z for the case with $\theta = 0^\circ$ and $\text{Co} = 0.03$.

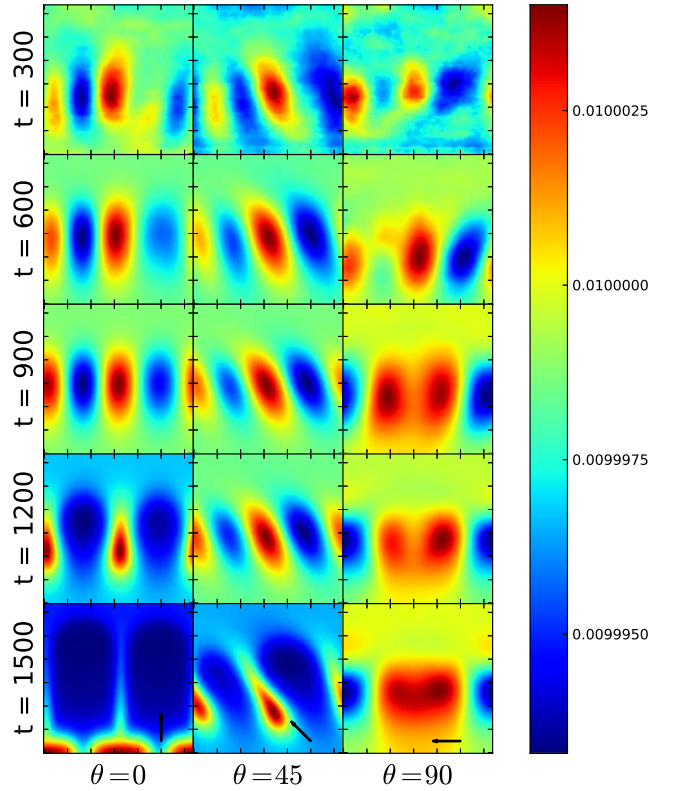


Fig. 9. Evolution of \bar{B}_y in the xz plane for $\Omega_0 = 0.01$ (corresponding to $\text{Co} = 0.006$) and $B_0/B_{\text{eq}0} = 0.1$ for $\theta = 0^\circ$, $\theta = 45^\circ$, and $\theta = 90^\circ$ near the time when the instability saturates. The direction of Ω is indicated in the last row.

y direction, which means that the inclination angles change only in discrete steps.

Returning to the case of positive values of Ω , but $\theta \neq 0$, we note a slow migration of the magnetic pattern to the left

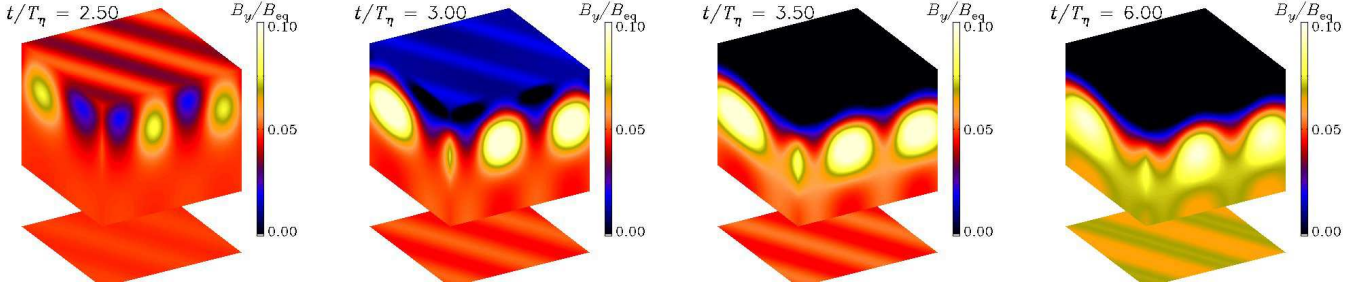


Fig. 10. Visualization of B_y on the periphery of the computational domain for 4 times (normalized in terms of T_η) during the nonlinear stage of the instability for $\theta = 0^\circ$ (corresponding to the equator) and $\text{Co} = 0.03$, corresponding to $2\Omega/\lambda_{*0} \approx 1.3$.

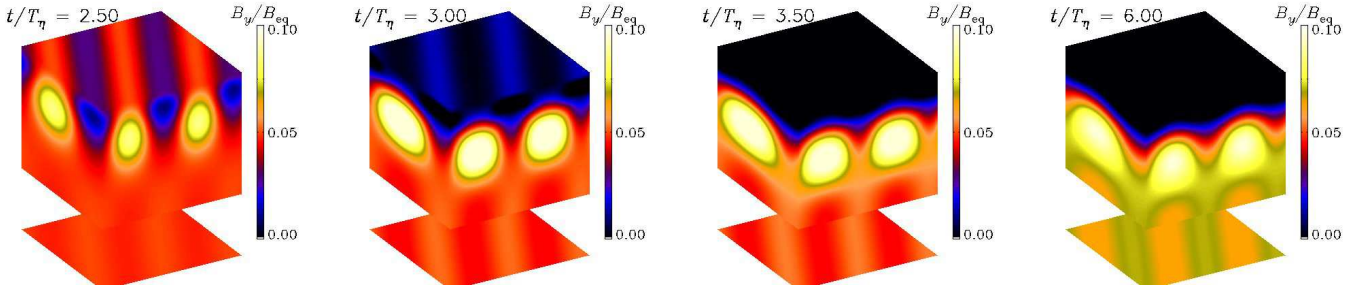


Fig. 11. Same as Figure 10, but for a negative value of Ω , i.e., $\text{Co} = -0.03$, corresponding to $2\Omega/\lambda_{*0} \approx -1.3$.

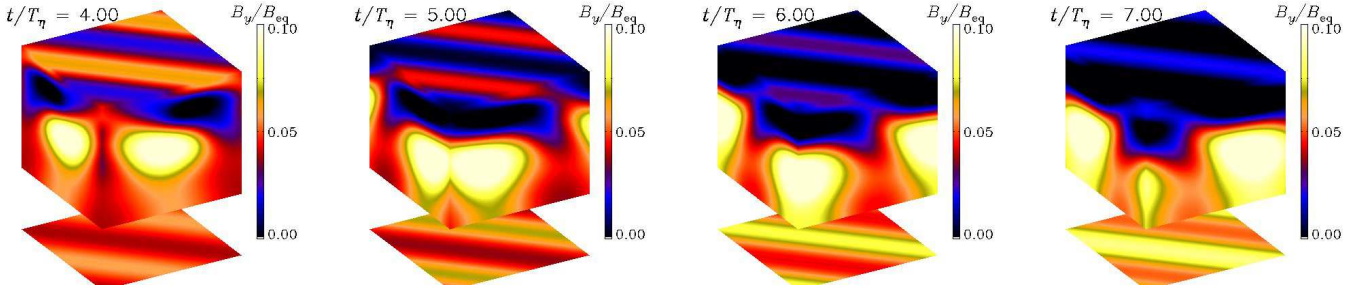


Fig. 12. Visualization of B_y on the periphery of the computational domain for 4 times (normalized in terms of T_η) during the nonlinear stage of the instability for $\theta = 45^\circ$ and $\text{Co} = 0.03$, corresponding to $2\Omega/\lambda_{*0} \approx 1.3$.

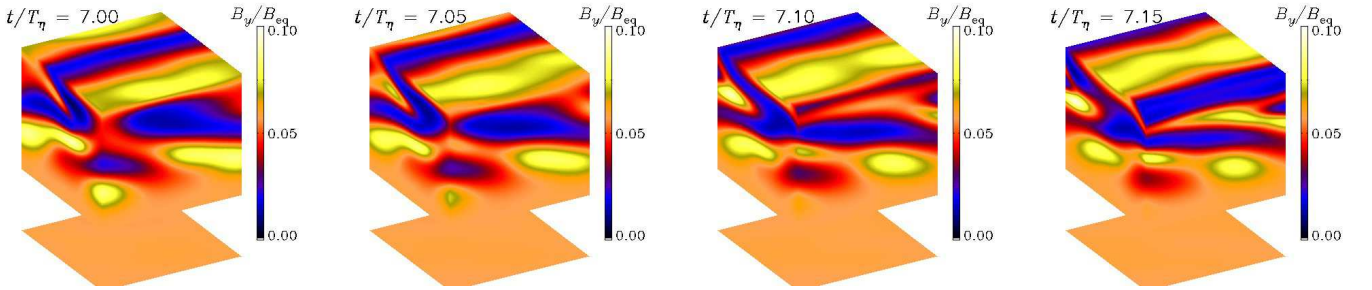


Fig. 13. Visualization of B_y on the periphery of the computational domain for 4 times (normalized in terms of T_η) during the nonlinear stage of the instability for $\theta = 90^\circ$ (corresponding to the equator) and $\text{Co} = 0.013$, corresponding to $2\Omega/\lambda_{*0} \approx 0.5$.

(here for $\theta = 45^\circ$), corresponding to poleward migration; see Figure 12. Note also that the field is tilted in the xy

plane. Finally, for $\theta = 90^\circ$ we see that the pattern speed corresponds to prograde motion; see Figure 13.

5. Conclusions

Although the physical reality of NEMPI has recently been confirmed by direct numerical simulations, its potential role for producing large-scale magnetic structures in the Sun is yet unclear and we are only now beginning to investigate its properties under conditions that are astrophysically important. Rotation is ubiquitous and clearly important in the Sun. The present work has now shown that already for rather slow rotation the instability is suppressed. This is rather surprising, because rotational effects normally become important only when Ω is comparable with the inverse turnover time, which is here defined as u_{rms}/k_f . The reason for this behavior is probably related to the fact that the growth rate of the instability does also not scale with the inverse turnover time, but that it is closer to the turbulent diffusive time, which is slower than the turnover time by the square of the scale separation ratio (Brandenburg et al., 2011). However, the present work now suggests that this is not quite right either and that the correct answer might be something in between. Indeed, we find here that growth rate and critical rotation rate are close to the parameter $\lambda_{*0} = \beta_* u_{\text{rms}}/H_\rho$, which can be smaller than the aforementioned turnover time by a factor of 40, although in solar convection, where $k_f H_\rho \approx 2.4$ (Kemel et al., 2012c) and $\beta_* \approx 0.23$ (Kemel et al., 2012b), it is estimated to be only ≈ 10 times smaller.

The suppression is strongest at the equator, where Ω is perpendicular to the direction of the gravity field, i.e., $\Omega \cdot \mathbf{g} = 0$, and less strong at the poles where Ω and \mathbf{g} are either parallel (south pole) or antiparallel (north pole). In the absence of rotation, the mean magnetic field only varies in a plane that is normal to the direction of the imposed mean magnetic field, i.e., $\mathbf{k} \cdot \mathbf{B}_0 = 0$, where \mathbf{k} stands for the wave vector of the resulting flow and magnetic field. However, in the presence of rotation the orientation of this plane changes such that now $\mathbf{k} \cdot (\mathbf{B}_0 + \lambda_{*0}^{-1} \Omega \times \mathbf{B}_0) = 0$.

At intermediate latitudes, i.e., with angles between Ω and \mathbf{g} in the range from 0° to 90° colatitude, the magnetic field pattern propagates slowly in the negative x direction, corresponding to poleward migration. The significance of this result is unclear. Had it been equatorward migration, one might have been tempted to associate this with the equatorward migration of the magnetic flux belts in the Sun from which sunspots emerge. On the other hand, at the equator this migration corresponds to prograde rotation which is a clear effect seen in the Sun where magnetic tracers are seen to rotate faster, i.e., in the prograde direction (Gizon et al., 2003). Even sunspots rotate faster than the gas itself (Pulkkinen & Tuominen, 1998).

One of our goals for future work is to verify the present findings in direct numerical simulations. Such simulations would also allow us to determine new turbulent transport coefficients, similar to the q_p parameter invoked in the present study. Such additional parameters yield new effects, some of which could be important for applications to the Sun.

Finally, let us comment of the issue of scale separation. As discussed above, in solar mixing length theory, the correlation length of the turbulent eddies is expected to scale with the pressure scale height such that $k_f H_\rho$ is constant and about 2.4 (Kemel et al., 2012c). Theoretical considerations have shown further that the growth rate of NEMPI is proportional to $k_f H_\rho$. Since rotation is known to decrease

the size of the turbulent eddies, i.e., to increase the value of k_f , one might be tempted to speculate that rotation could even enhance the growth rate of NEMPI. However, in view of the present results, this seems now unlikely.

Acknowledgements. Illa R. Losada was supported by PhD Grant ‘Beca de Investigación CajaCanarias para Postgraduados 2011’. This work was supported in part by the European Research Council under the AstroDyn Research Project No. 227952 by the National Science Foundation under Grant No. NSF PHY05-51164 (AB), by COST Action MP0806, by the European Research Council under the Atmospheric Research Project No. 227915 and by a grant from the Government of the Russian Federation under contract No. 11.G34.31.0048 (NK, IR). We acknowledge the allocation of computing resources provided by the Swedish National Allocations Committee at the Center for Parallel Computers at the Royal Institute of Technology in Stockholm and the National Supercomputer Centers in Linköping.

References

- Brandenburg, A. 2001, ApJ, 550, 824
- Brandenburg, A., & Dobler, W. 2002, Comp. Phys. Comm., 147, 471
- Brandenburg, A., & Subramanian, K. 2005, Phys. Rep., 417, 1
- Brandenburg, A., Kemel, K., Kleeorin, N., Mitra, D., Rogachevskii, I. 2011, ApJ, 740, L50
- Brandenburg, A., Kemel, K., Kleeorin, N., Rogachevskii, I. 2012, ApJ, 749, 179
- Brandenburg, A., Kleeorin, N., Rogachevskii, I. 2010, Astron. Nachr., 331, 5
- Brandenburg, A., Nordlund, Å., Pulkkinen, P., Stein, R.F., & Tuominen, I. 1990, A&A, 232, 277
- Gizon, L., Duvall Jr, T. L., & Schou, J. 2003, Nature, 421, 43
- Käpylä, P. J., Brandenburg, A., Kleeorin, N., Mantere, M. J., & Rogachevskii, I. 2012, MNRAS, 422, 2465
- Kemel, K., Brandenburg, A., Kleeorin, N., & Rogachevskii, I. 2012, Astron. Nachr., 333, 95
- Kemel, K., Brandenburg, A., Kleeorin, N., Mitra, D., & Rogachevskii, I. 2012, Solar Phys., arXiv:1112.0279, DOI:10.1007/s11207-012-9949-0
- Kemel, K., Brandenburg, A., Kleeorin, N., Mitra, D., & Rogachevskii, I. 2012, Solar Phys., arXiv:1203.1232, DOI:10.1007/s11207-012-0031-8
- Kleeorin, N., Rogachevskii, I. 1994, Phys. Rev. E, 50, 2716
- Kleeorin, N., Mond, M., Rogachevskii, I. 1993, Phys. Fluids B, 5, 4128
- Kleeorin, N., Mond, M., Rogachevskii, I. 1996, A&A, 307, 293
- Kleeorin, N.I., Rogachevskii, I.V., Ruzmaikin, A.A. 1989, Sov. Astron. Lett., 15, 274
- Kleeorin, N.I., Rogachevskii, I.V., Ruzmaikin, A.A. 1990, Sov. Phys. JETP, 70, 878
- Krause, F., & Rädler, K.-H. 1980, Mean-field magnetohydrodynamics and dynamo theory (Pergamon Press, Oxford)
- Moffatt, H.K. 1978, Magnetic field generation in electrically conducting fluids (Cambridge University Press, Cambridge)
- Parker, E.N. 1966, ApJ, 145, 811
- Parker, E.N. 1979, Cosmical magnetic fields (Oxford University Press, New York)
- Pulkkinen, P., & Tuominen, I. 1998, A&A, 332, 748
- Priest, E.R. 1982, Solar Magnetohydrodynamics (D. Reidel Publ. Co., Dordrecht)
- Rogachevskii, I., Kleeorin, N. 2007, Phys. Rev. E, 76, 056307
- Sur, S., Brandenburg, A., & Subramanian, K. 2008, MNRAS, 385, L15
- Tserkovnikov, Y. A. 1960, Sov. Phys. Dokl., 5, 87
- Vitense, E. 1953, Z. Astrophys., 32, 135
- Zeldovich, Ya. B., Ruzmaikin, A. A., Sokoloff, D. D. 1983, Magnetic fields in astrophysics (Gordon & Breach, New York)

\$Header: /var/cvs/brandenb/tex/illa/NEMPI_rotation/paper.tex,v 1.107